

Lyman-alpha Radiation Pressure in the Heliosphere: Results from a 3D Monte Carlo Radiative Transfer Simulation

This content has been downloaded from IOPscience. Please scroll down to see the full text.

2015 J. Phys.: Conf. Ser. 642 012007

(<http://iopscience.iop.org/1742-6596/642/1/012007>)

View [the table of contents for this issue](#), or go to the [journal homepage](#) for more

Download details:

IP Address: 207.157.71.69

This content was downloaded on 16/11/2015 at 16:50

Please note that [terms and conditions apply](#).

Lyman-alpha Radiation Pressure in the Heliosphere: Results from a 3D Monte Carlo Radiative Transfer Simulation

B Fayock¹, G P Zank^{1,2}, J Heerikhuisen^{1,2}, C R Gilbert³ and K Scherer⁴

¹ Center for Space Plasma and Aeronomic Research, University of Alabama in Huntsville, Huntsville, AL 35805, USA

² Department of Space Science, University of Alabama in Huntsville, Huntsville, AL 35805, USA

³ Department of Physics, Georgia Technical Institute, Atlanta, GA, 30332, USA

⁴ Institut für Experimentalphysik II, Ruhr-Universität Bochum, Universitätsstraße 150, Bochum, Germany

E-mail: brian.fayock@gmail.com, garyp.zank@gmail.com, jacob.heerikhuisen@uah.edu, cgilbert7@gatech.edu, kls@tp4.rub.de

Abstract. Global models of the heliosphere and its interaction with the local interstellar medium have evolved to fit spacecraft observations since the beginning of their development. It is now understood that neutral hydrogen plays a very important role in the modification of the shape and location of the heliopause. Comparisons of simulations to observations have often led to the need for a more accurate treatment of a particular process. We bring attention to a long-held assumption that radiation pressure on neutral hydrogen atoms due to Lyman-alpha absorption and emission falls off with heliocentric distance at the same rate as solar gravitation. These have generally been combined into a single term. Through our Monte Carlo simulation of Lyman-alpha radiative transfer in the heliosphere, we show that the radiation pressure 1) falls off at a slower rate than r^{-2} and 2) is not isotropic. We find that the radiation pressure in the upwind direction falls off with heliocentric distance with a power of approximately -1.80 between ~ 6 and 75 AU, while the downwind direction falls off with a much slower rate and more variability over heliocentric distance. We discuss our methods and results as well as the implications below.

1. Introduction

Partially ionized interstellar gas and dust constitute the bulk of the galactic medium through which the sun travels and with which the solar wind interacts, resulting in a complex structure called the heliosphere. The general structure of this interaction is shown in Figure 1. As the plasma and magnetic field of the local interstellar medium (LISM) comes to a pressure balance with that of the solar wind at the heliopause, the neutral hydrogen (H) atoms of the LISM are subject to charge-exchange collisions with plasma and elastic collisions with other H atoms, but do not interact directly with the magnetic field, and thus are able to penetrate into the heliosphere to within several AU of the sun. From the time H atoms come into the picture from the LISM, the charge-exchange collisions with protons create new H atoms with properties of



the local plasma distribution. This results in a different population of H atoms for each region, which provides the basis of their separation into components as well as their naming, also shown in Figure 1. Component 0 refers to the neutral H atoms that come directly from the LISM, while neutral components 1, 2, and 3 are created in the outer heliosheath, inner heliosheath, and supersonic solar wind, respectively. We refer the reader to several reviews for a detailed description of the heliosphere and various physical processes [1, 2, 3, 4].

Global models of the heliosphere have been in development for decades. While the interaction of the plasma and magnetic field of both the solar wind and the interstellar medium is responsible for the formation of the heliospheric boundaries, neutral H atoms have been shown to have a significant effect on its overall structure [5, 6]. Therefore, global models must be able to incorporate all interactions relevant to neutral H in order to accurately describe their inclusion. A few of the first models that were able to include neutral H self-consistently were the Monte Carlo code of Ref. [7] and the series of multi-fluid codes by Refs. [8, 9, 10], where coupling to the plasma populations was achieved through source and loss terms.

Since the inception of the self-consistent models, the presence of neutral H has been and

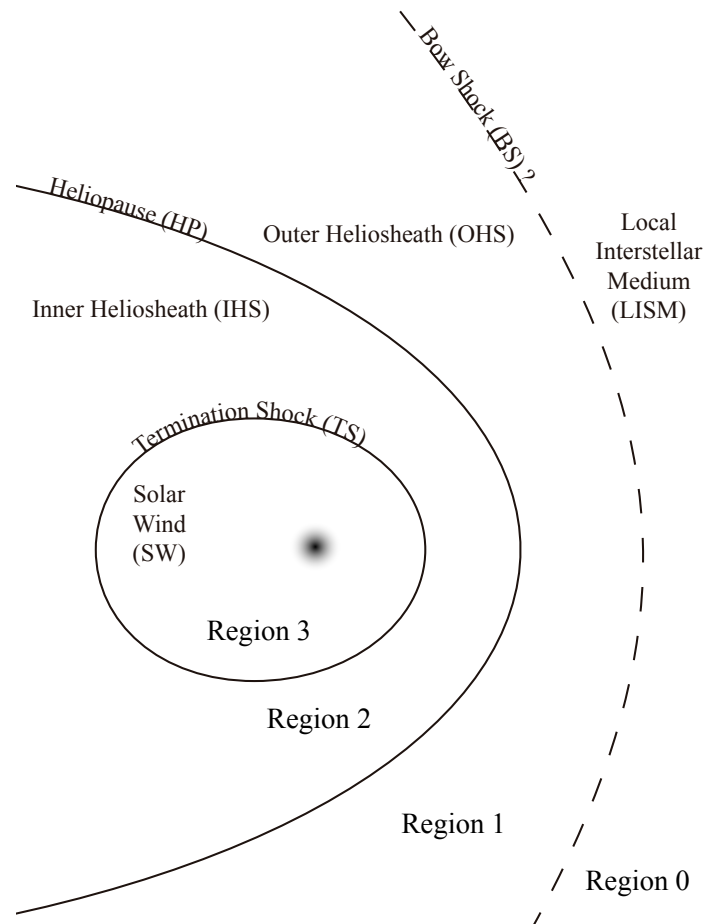


Figure 1. Schematic of the heliosphere showing the four separate regions: region 0 - the local interstellar medium (LISM), region 1 - the outer heliosheath (OHS), region 2 - the inner heliosheath (IHS), and region 3 - the supersonic solar wind (SW).

continues to be studied extensively from both kinetic and multi-fluid perspectives. Some studies with multi-fluid models include, but are certainly not limited to, galactic cosmic ray transport [11], Rayleigh-Taylor and Kelvin-Helmholtz instabilities [12, 13, 14], the coupling of solar wind and interstellar magnetic fields [15, 16, 17], and solar rotation and activity cycle [18, 19]. While the incorporation of time-dependent effects are natural for fluid models, the assumption of being able to treat each population as having a Maxwellian distribution can lead to large deficiencies in the characterization of kinetic energy of neutral H, especially within regions 2 and 3. Differences between the resulting velocity distributions of each region can be seen in Ref. [20], which compares the various structural effects on the heliosphere between kinetic and multi-fluid treatments of 4 neutral H components using the same interstellar parameters.

Further work with kinetic models used κ distributions to describe the velocity distributions of heliosheath protons with the intention of simulating the production and detection of energetic neutral atoms (ENAs) [2, 21, 22, 23] that would be detected by NASA's Interstellar Boundary Explorer [24]. Shortly after launch, the detection of an unexpected and interesting "ribbon" feature within the data required the inclusion of secondary ENA production just outside the heliopause [25], which result from a more complex description of pickup ions in the heliosheath. Due to the influence of the interstellar magnetic field on these secondary ENAs, this led to further investigation of the interstellar parameters with a focus on the strength and orientation of the magnetic field [26, 27] as well as further investigations of pickup ions throughout the heliosphere [2, 28, 29] and a more recent study of solar cycle effects [30].

While there has been substantial progress in the development of global models for both multi-fluid and kinetic treatments of neutral H, there is yet another assumption that requires more attention. Within nearly all works mentioned above, radiation pressure and solar gravitation have been combined into a single term in the treatment of influential forces on neutral H atoms as a ratio, μ . Although variation of this parameter has been used to incorporate the time-varying solar flux, radiation pressure has been assumed to fall off with distance as r^{-2} . We show here through the simulation of Lyman-alpha radiation in the heliosphere using a 3D Monte Carlo radiative transfer code [31] that this assumption is no longer valid. We briefly outline our methods below and discuss the results of radiation pressure as well as their implications for modeling of the heliosphere.

2. Radiative Transfer Code

Lyman-alpha radiation is constantly being absorbed and emitted by every neutral H atom throughout the heliosphere. The probability of absorption depends strongly on the properties of the neutral H distribution. Therefore, observations of the emitted photons can reveal information about the surrounding H distribution and subsequently imply several very important properties about the local plasma distribution. This ultraviolet line has been and continues to be observed by several space-based missions. Our particular interests are the deep-space missions that have been able to measure the trend of Lyman-alpha intensity over an increasing heliocentric distance: *Voyager* [32] and *Pioneer* [33].

In order to study Lyman-alpha radiation in the heliosphere, we developed a 3D Monte Carlo radiative transfer code [31] to simulate the Lyman-alpha backscatter as would be seen by the ultraviolet detectors on board these deep-space missions throughout the heliosphere. This code utilizes a static neutral hydrogen distribution resulting from a 3D MHD-kinetic neutral model of the heliosphere [20, 21]. Within this static code, the LISM is set with the following properties: neutral H density of $0.15 \text{ atoms cm}^{-3}$, $0.05 \text{ protons cm}^{-3}$, 6527 K, and the incoming H flow directed along the x-axis at 26.4 km s^{-1} . The solar wind is set in solar minimum conditions according to the following parameters at 1 AU: a proton density of 7.0 cm^{-3} , velocity of 400 km s^{-1} , and temperature of 100,000 K below a solar equatorial latitude of 35° and 2.6 cm^{-3} , 800 km s^{-1} , and 260,000 K, respectively, above. While the LISM parameters thus far are generally

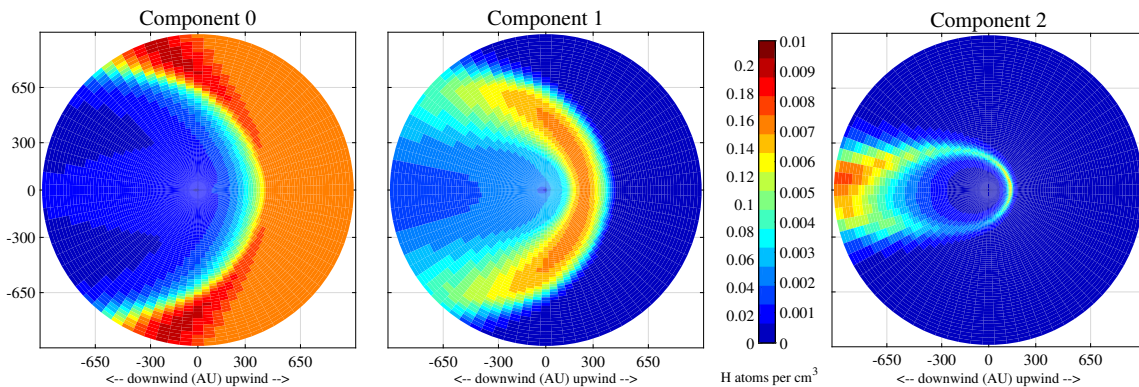


Figure 2. Three components of density for regions 0, 1, and 2 of the neutral hydrogen distribution in the heliosphere. This background data is presented in the Ecliptic plane.

axisymmetric along the x-axis, there is an asymmetry in the magnetic field as its origin is shifted 60° above the Ecliptic plane from the upwind direction. The distribution of density for the first three components of H can be seen in Figure 2. The model also yields the temperature and a velocity vector for each neutral H component.

Our radiative transfer code simulates the absorption and emission of millions of photons within this static neutral hydrogen distribution (without feedback), treating absorption and emission as separate processes with a combination of frame rotations and conservation of momentum. From each interaction we are able to determine the total momentum transferred to the H atoms in the radial direction. The code follows one photon at a time, which is generated only from the sun. Each photon is randomly assigned a direction and a frequency within a range that corresponds to H Doppler shifts within $\pm 120 \text{ km s}^{-1}$. This range covers the H velocity distributions for components 0, 1, and 2. The frequencies are also chosen to follow the self-reversed profile developed by Refs. [34, 35]. The same profile is used uniformly over the entire surface so no polar variation is considered here. Each photon is then subject to absorption and subsequent emission until eventual exit from the computational grid.

The absorption is considered as the probability that a single photon will be absorbed by one of the three components of H-atoms within a particular grid cell, each of which are described by a Maxwellian distribution, resulting in the absorption cross section [36]

$$\sigma = \frac{\sqrt{\pi} q_e^2 f_{12}}{m_e c \Delta v_D} \exp \frac{(\nu' - \nu_{L\alpha})^2}{\Delta v_D^2}, \quad (1)$$

where f_{12} is the oscillator strength of the transition (0.4162 for the Lyman-alpha line), q_e is the charge of an electron, $\nu_{L\alpha}$ is the Lyman-alpha frequency, $\Delta v_D = (\nu_{L\alpha}/c) \sqrt{2k_B T/m_H}$ is the thermal Doppler width, and $\nu' = \nu [1 - (\vec{v}_H \cdot \vec{v}_c)/(c^2)]$ is the Doppler-shifted frequency of the photon in the frame of a H atom having the local bulk velocity of the component in question (each component is calculated separately). The dot product in the calculation of the relative frequency is complicated by the fact that the two vectors are not defined in the same reference frame. The hydrogen vector is defined in Cartesian coordinates in the solar frame, and the velocity of the photon is in its own frame that depends on its position within the solar frame. This issue is solved with frame rotations using quaternions [37] and is described in detail in Ref. [31]. The temperature here is treated homogeneously and is derived from the average kinetic energy associated with random velocities of the hydrogen atoms.

The probability of absorption is then calculated as the complement of the probability of no absorption, which is ultimately described as

$$p_s = 1 - \exp[-s(\rho_0\sigma_0 + \rho_1\sigma_1 + \rho_2\sigma_2)], \quad (2)$$

where s is the distance traveled by the photon since its previous interaction or grid-cell boundary crossing and ρ is the density of a particular component. This probability is then compared to a uniformly-generated random variable, t_r between 0 and 1. If $t_r < p_s$, the photon is absorbed. Otherwise, it continues on its path to the boundary of the next grid cell.

Upon absorption, an emission angle is randomly generated from an approximate inverse function [38] of a mixed-dipole phase function [39] in the frame of the H atom. While within the H atom frame, an emission frequency is calculated based on the possibility of either radiative decay or immediate emission, for an absorbed photon with energy greater or less than that of Lyman alpha, respectively. With this information, we are able to calculate the radial contribution of momentum that has been transferred to the hydrogen atom upon absorption as well as the momentum lost to the photon upon emission.

To complete the interaction, we must consider the resulting change in momentum of the H atom before calculating the frequency of the photon in the solar frame. The change in momentum of the H atom is calculated in the photon velocity frame and added to the original velocity, which is then multiplied by the new emission direction as a dot product to find the relative velocity of the hydrogen atom in the new emission frame, thereby allowing for the calculation of the frequency of the emitted photon in the solar frame. The emitted photon is then subject to further absorption and subsequent emission (without limitation) until it exits the computational grid. This process of photon generation, absorption, and emission is repeated for millions of photons while the statistics of each interaction are stored in a 5-dimensional (5D) array, including frequency, direction, and three dimensions of space for the entire computational grid.

3. Direct Results

In order to convince the reader of the reliability of our radiation pressure results, we first compare our simulations of photon backscatter to spacecraft observations. In Figures 3 and 4, we present the direct results from the current work, which has been updated since our first results [40], and compare to *Voyager 1* and *Pioneer 10* data that has been previously reduced by Doyle T. Hall in his thesis in 1992 [41]. In these Figures, we show three values calculated directly from our statistical collection (emission, collection, and total time spent) and one post-processed result.

The statistical values that we present here are rather straightforward. Upon each absorption, the calculation described above is performed and results in an emitted photon. This emitted photon is logged in the appropriate 5D bin, and a new calculation for the probability of absorption must take place. If this photon is then determined to be absorbed within the distance to the next grid cell, the photon is logged for absorption. Otherwise, the photon makes it to the next grid cell, where the calculation is performed again. Whether the photon is absorbed or not, the distance between the current and previous location is added to the running total in the appropriate 5D bin. While this value is logged as distance, the constant value of the speed of a photon allows a direction relationship to the time required to cross that distance. This total value is treated as the probability of a photon being detected. All statistics are then divided by volume to give their value per unit volume. While it is impossible to generate a realistic number of photons within the program, it is the relative value distributed throughout the grid space that we focus on here. As such, each of the statistical values, as well as the spacecraft data, are normalized to 1.0 at approximately 15 AU.

At each point that a photon statistic is logged, its directional velocity is used to determine the appropriate angular bin. In this particular run, there were three possible angular bins, defined by the local polar angle with respect to the radial position vector. An angle of zero is defined to be parallel to the radial vector (anti-solar), while 180° is antiparallel (solar). There are two

cones that define the boundaries of these three angular bins such that each is of equal solid angle. There is one anti-solar cone, one cone pointed in the solar direction, and one region for all lateral angles in between. The values shown in Figures 3 and 4 are the results for the angular bin that is directed towards the sun, resulting in backscatter emission, anti-solar collection, total time spent traveling towards the sun, and the post-processed calculation, where the backscatter emission is integrated along the anti-solar line of sight. These values generally follow a similar slope, with the backscatter emission having more variability because it is more dependent on the local parameters of the neutral H distribution.

In terms of our results for radiation pressure, it is more important that the *Voyager 1* results in Figure 4 are acknowledged to match extremely well. Since this data set only goes out to ~ 40 AU, we can only say with certainty that the results match up to 40 AU, but this is sufficient to establish our point. Our results for radiation pressure can be seen for the upwind and downwind directions in Figures 5 and 6. We plot several values of a constant exponential power for each plot to show how the trends compare to that of solar gravitation. We show linear fits to a single group of points for *Voyager 1* and several groups of points for *Pioneer 10* along with the standard error of the resulting values for each slope. We have not considered uncertainty in either the neutral H data nor the resulting points themselves. The uncertainties in the resulting values are plotted as gray triangles in Figures 5 and 6, which we consider to be very small relative to the line fit and uncertainty calculations and would have no change in our conclusions.

For the upwind direction, the trend of radiation pressure over heliocentric distance between 4.55 and 73.6 AU follows a power of -1.8068 ± 0.0054 , which then slowly changes to a steeper slope up to the heliopause, where it transitions rather quickly to a slope that is steeper than -3.00 throughout the hydrogen wall and the remainder of the computational grid at ~ 1000 AU. The trends in the downwind direction are -1.2126 ± 0.0185 from 2.88 to 18.5 AU and -1.5256 ± 0.0118 from 14.9 to 55.2 AU after which the slope transitions to a power of -2.2287 ± 0.0186 from 88.5 up to nearly 200 AU, where it drops even further over a few tens of AU to -2.6444 ± 0.0052 out to the edge of the computational grid.

4. Discussion

We have presented the results of our 3D Monte Carlo radiative transfer simulation of Lyman-alpha in the heliosphere using a static background of a neutral hydrogen distribution described

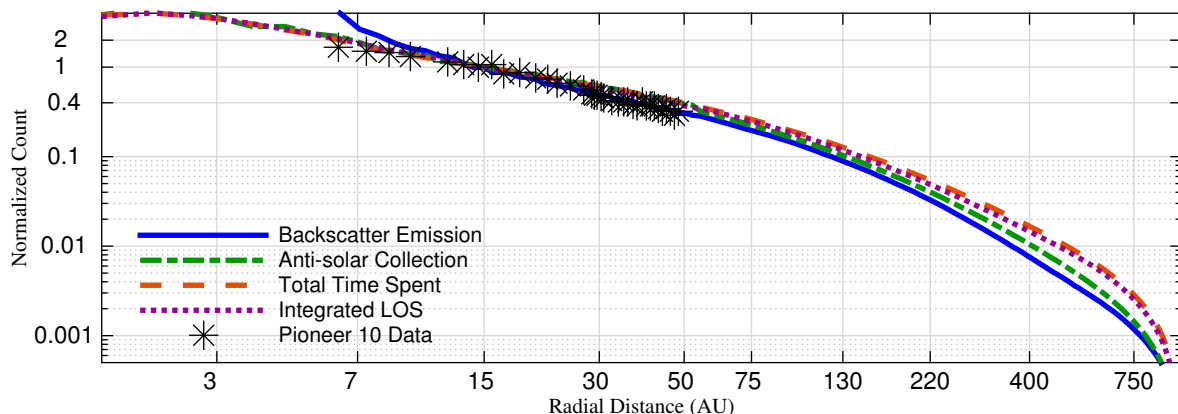


Figure 3. Direct results for *Pioneer 10*. Backscatter emission is the solid blue line; anti-solar collection is the dash-dotted green line; total time spent is the dashed orange line; post-processed integrated line-of-sight is the dotted purple line. The *Pioneer 10* data is shown as asterisks.

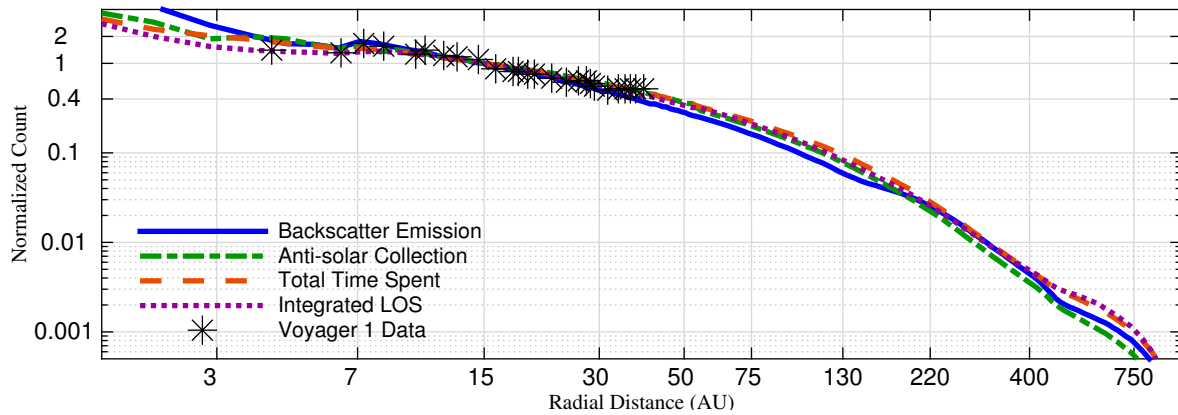


Figure 4. Direct results for *Voyager 2*. Plotted with the same representation as Figure 3.

by three separate components. Our method treats the absorption and subsequent emission of Lyman-alpha photons by H atoms as separate processes. We have shown by comparison that our results are able to reproduce spacecraft data rather well, providing support for the reliability of our radiation pressure results.

We have come to two main conclusions with these results. One conclusion is that the radiation pressure falls off, not as r^{-2} , but at a slower rate within most of region 3 with a variety of slopes elsewhere. This rate is not very much slower in the upwind direction (-1.8068), but is significantly slower in the downwind direction (-1.2126), which brings us to our second conclusion. The radiation pressure is certainly not isotropic. We can see that the results are rather consistent within 75 AU in the upwind direction, but surprisingly much more variable in the downwind direction.

There may be several aspects of the heliosphere that influence the radiation pressure in the manner that we see. We can certainly say that multiple scattering is incredibly important and provides a much longer lasting source of Lyman alpha radiation in the outer heliosphere than that resulting from an optically thin solution. We also think that the increasing density of neutral H in the upwind direction aids in the decrease in radiation pressure due to an increasing probability of absorption and emission, but the parabolic shape of this increase that culminates

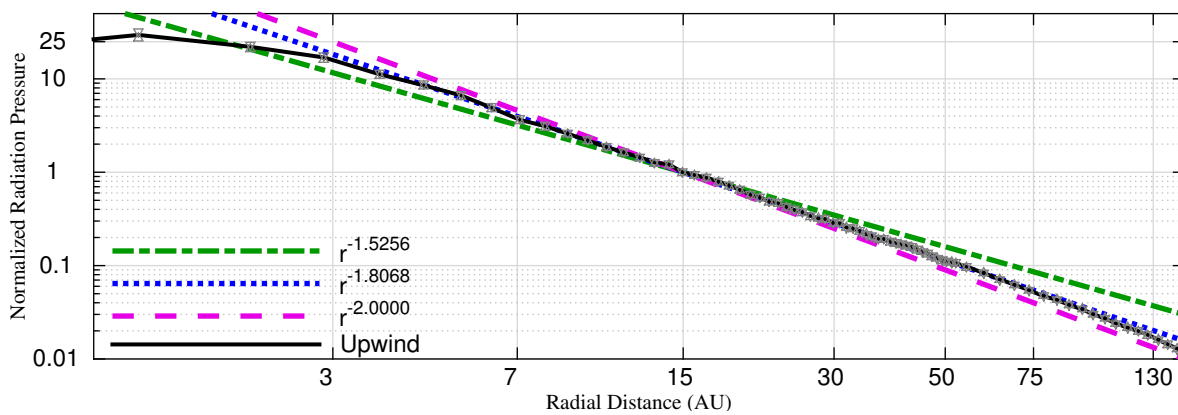


Figure 5. Radiation pressure in the downwind direction. Results show the line fit between 4.55 and 73.6 AU as well as two reference slopes, where -2.00 corresponds to the slope for solar gravitation and -1.5256 is one of the fits for the downwind direction.

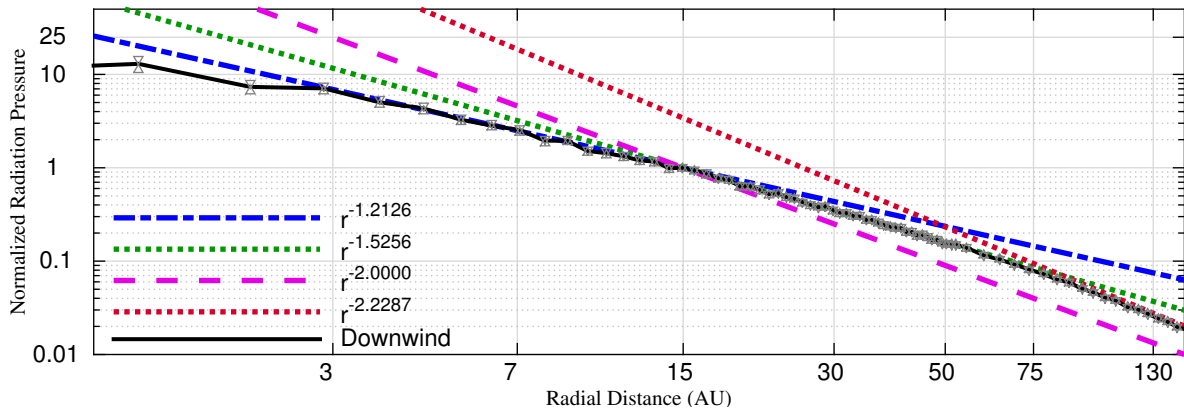


Figure 6. Radiation pressure in the upwind direction. Results show three line fits: one from 2.88 to 18.5 AU, one from 14.9 to 55.2 AU for a little overlap, and another from 88.5 to nearly 200 AU. The reference slope of -2.00 is also shown.

at the heliopause may act as a “focusing beam” that redirects the Lyman alpha toward the downwind direction, providing a much more sustainable source of radiation pressure in the inner heliosphere.

Since the initial heliospheric models describing neutral hydrogen in the 1970’s, radiation pressure has been considered to fall off as r^{-2} and combined with solar gravitation as a single parameter, generally in the literature as μ or the ratio of radiation pressure to gravitational force from the sun. Variations of this parameter have been the source of much discussion for heliospheric models, even to this day, along the lines of its variation with solar cycle activity. No matter what value is used for μ , the effect always produces a relation that falls off as r^{-2} , which is not a realistic assumption. We consider the results presented here to be significant, supporting the idea that the heliosphere is not optically thin to Lyman alpha.

There have been a number of radiative transfer studies conducted in the past [38, 41, 42, 43, 44] as well as continuations of those works. However, one or more issues have prevented each from resulting in a match to multiple spacecraft data. One idea that has generally been incorporated is the use of a single function [45] to describe the redistribution of a photon’s frequency from absorption to emission by a H atom in the laboratory frame. It is our understanding that this equation was developed for an elegant analytical result, but is not quite necessary for computational calculations. We also treat photons kinetically as opposed to the other option of treating the radiation as a fluid through iterative solutions. In that case, multiple scattering is difficult to handle, especially when the scattering phase function is not isotropic. Another difference between our results and others mention above is the background neutral H distribution. While we have not tested our code on distributions from other groups, our global heliospheric model has been quite successful in comparisons to several types of spacecraft observations. One or more of these differences may be responsible for the agreement of our results with ultraviolet data where other works have been unsuccessful.

5. Conclusions

Heliospheric models have assumed that radiation pressure exerted on neutral H falls off with heliocentric distance at the same rate as that of solar gravitation since their first conception. Through our Monte Carlo simulation of Lyman-alpha radiative transfer in the heliosphere, we are able to statistically calculate the radially-directed momentum that is transferred to neutral H during absorption and emission. We have shown the results for the upwind and downwind

directions.

While our calculations have been made within a static heliospheric model under solar minimum conditions, the simple result that the radiation pressure is not isotropic provides enough of an argument to include a more detailed radiation pressure model in the treatment of neutral hydrogen. However, we consider our comparison to spacecraft data to provide the support necessary to conclude that radiation pressure generally falls off slower than r^{-2} except within the heliopause, where it can fall off more rapidly, and cannot be combined into a single parameter with solar gravitation.

Acknowledgments

This work was partially supported by NASA grants NNX08AJ33G, Subaward 37102-2, NNX09AG70G, NNX09AG63G, NNX09AJ79G, NNG05EC85C, NNX09AP74A, NNX10AE46G, NNX09AW45G, NNH09AM47I, and Subcontract A991132BT, and NSF grant ATM-0904007.

References

- [1] Zank G P 1999 Interaction of the solar wind with the local interstellar medium: a theoretical perspective *Space Sci. Rev.* **89** 413
- [2] Zank G P, Heerikhuisen J, Pogorelov N V, Burrows R and McComas D 2010 Microstructure of the heliospheric termination shock: implications for energetic neutral atom observations *Astrophys. J.* **708** 1092
- [3] Zank G P, Heerikhuisen J, Wood B E, Pogorelov N V, Zirnstein E and McComas D 2013 Heliospheric structure: the bow wave and the hydrogen wall *Astrophys. J.* **763** 20
- [4] Izmodenov A A, Malama Y G, Ruderman M S, Chalov S V, Alexashov D B, Katushkina O A, and Provornikova E A 2009 Kinetic-Gasdynamic Modeling of the Heliospheric Interface *Space Sci. Rev.* **146** 329
- [5] Zank G P, Müller H R and Wood B E 2001 The interaction of the solar wind and stellar winds with the partially ionized interstellar medium *Phys. Plasmas* **8** 2385
- [6] Zank G P and Müller H R 2003 The dynamical heliosphere *J. Geophys. Res. (Space Phys.)* **108** 1240
- [7] Baranov V B and Malama Y G 1993 Model of the solar wind interaction with the local interstellar medium: numerical solution of self-consistent problem *J. Geophys. Res.* **98** 15157
- [8] Pauls H L, Zank G P and Williams L L 1995 Interaction of the solar wind with the local interstellar medium *J. Geophys. Res.* **100** 21595
- [9] Zank G P, Pauls H L, Williams L L and Hall D T 1996 Interaction of the solar wind with the local interstellar medium: a multi fluid approach *J. Geophys. Res.* **101** 21639
- [10] Pauls H L and Zank G P 1997 Interaction of a nonuniform solar wind with the local interstellar medium: 2. a two-fluid model *J. Geophys. Res.* **102** 19779
- [11] Florinski V, Zank G P and Pogorelov N V 2003 Galactic cosmic ray transport in the global heliosphere *J. Geophys. Res. (Space Phys.)* **108** 1228
- [12] Florinski V, Zank G P and Pogorelov N V 2005 Heliopause stability in the presence of neutral atoms: Rayleigh-Taylor dispersion analysis and axisymmetric MHD simulations *J. Geophys. Res. (Space Phys.)* **110** 7104
- [13] Zank G P 1999 *AIP Conf. Ser.* vol 471, ed S R Habbal *et al* (Melville, NY: AIP), p 783
- [14] Avinash K, Zank G P, Dasgupta B and Bhadoria S 2014 Instability of the heliopause driven by charge exchange interactions *Astrophys. J.* **791** 102
- [15] Pogorelov N V and Zank G P 2005 Coupling of the interstellar and interplanetary magnetic fields at the heliospheric interface: the effect of neutral hydrogen atoms *Adv. Space Res.* **35** 2055
- [16] Pogorelov N V, Zank G P and Ogino T 2006 Three-dimensional features of the outer heliosphere due to coupling between the interstellar and interplanetary magnetic fields. II. the presence of neutral hydrogen atoms *Astrophys. J.* **644** 1299
- [17] Pogorelov N V, Heerikhuisen J, Zank G P and Borovikov S N 2009 Influence of the interstellar magnetic field and neutrals on the shape of the outer heliosphere *Space Sci. Rev.* **143** 31
- [18] Pogorelov N V, Borovikov S N, Zank G P and Ogino T 2009 Three-dimensional features of the outer heliosphere due to coupling between the interstellar and interplanetary magnetic fields. III. the effects of solar rotation and activity cycle *Astrophys. J.* **696** 1478
- [19] Washimi H, Zank G P, Hu Q, Tanaka T, Munakata K and Shinagawa H 2011 Realistic and time-varying outer heliospheric modeling *Mon. Not. Roy. Astron. Soc.* **416** 1475

- [20] Heerikhuisen J, Florinski V and Zank G P 2006 Interaction between the solar wind and interstellar gas: a comparison between Monte Carlo and fluid approaches *J. Geophys. Res. (Space Phys.)* **111** 6110
- [21] Heerikhuisen J, Pogorelov N V, Florinski V, Zank G P and le Roux J A 2008 The effects of a κ -distribution in the heliosheath on the global heliosphere and ENA flux at 1 AU *Astrophys. J.* **682** 679
- [22] Heerikhuisen J and Pogorelov N V 2009 Detecting neutral atoms from beyond the heliopause with Interstellar Boundary Explorer *Astrophys. J.* **695** L58
- [23] Zirnstein E J, Heerikhuisen J and Pogorelov N V 2012 *AIP Conf. Ser., Space Weather: The Space Radiation Environment* vol 1500, ed Q Hu *et al* (Melville, NY: AIP), p 262
- [24] McComas D J *et al* 2009 IBEX-Interstellar Boundary Explorer *Space Sci. Rev.* **146** 11
- [25] Heerikhuisen J, Pogorelov N V, Zank G P, Crew G B, Frisch P C, Funsten H O, Janzen P H, McComas D J, Reisenfeld D B and Schwadron N A 2010 Pick-up ions in the outer heliosheath: a possible mechanism for the Interstellar Boundary Explorer ribbon *Astrophys. J.* **708** L126
- [26] Heerikhuisen J and Pogorelov N V 2011 An estimate of the nearby interstellar magnetic field using neutral atoms *Astrophys. J.* **738** 29
- [27] Heerikhuisen J, Zirnstein E J, Funsten H O, Pogorelov N V and Zank G P 2014 The effect of new interstellar medium parameters on the heliosphere and energetic neutral atoms from the interstellar boundary *Astrophys. J.* **784** 73
- [28] Zirnstein E J, Heerikhuisen J, Zank G P, Pogorelov N V, McComas D J and Desai M I 2014 Charge-exchange coupling between pickup ions across the heliopause and its effect on energetic neutral hydrogen flux *Astrophys. J.* **783** 129
- [29] Zank G P, Hunana P, Mostafavi P and Goldstein M L 2014 Pickup ion mediated plasmas. I. basic model and linear waves in the solar wind and local interstellar medium *Astrophys. J.* **797** 87
- [30] Zirnstein E J, Heerikhuisen J, Pogorelov N V, McComas D J and Dayeh M A 2015 Simulations of a dynamic solar cycle and its effects on the Interstellar Boundary Explorer ribbon and globally distributed energetic neutral atom flux *Astrophys. J.* **804** 5
- [31] Fayock B 2013 *Analysis of solar lyman-alpha scattering in the heliosphere* Ph.D. thesis University of Alabama in Huntsville ([open access](http://open.access.dissexpress.umi.com) [dissexpress.umi.com](http://open.access.dissexpress.umi.com))
- [32] Broadfoot A L, Sandel B R, Shemansky D E, Atreya S K, Donahue T M, Moos H W, Bertaux J L, Blamont J E, Ajello J M and Strobel D F 1977 Ultraviolet spectrometer experiment for the Voyager mission *Space Sci. Rev.* **21** 183
- [33] Carlson R W and Judge D L 1974 Pioneer 10 ultraviolet photometer observations at Jupiter encounter *J. Geophys. Res.* **79** 3623
- [34] Tarnopolski S 2007 *Expected distribution of interstellar deuterium in the heliosphere* (in Polish) Ph.D. thesis Space Research Centre PAS
- [35] Tarnopolski S and Bzowski M 2009 Neutral interstellar hydrogen in the inner heliosphere under the influence of wavelength-dependent solar radiation pressure *Astron. Astrophys.* **493** 207
- [36] Rybicki G B and Lightman A P 1979 *Radiative Processes in Astrophysics* (New York: Wiley-Interscience)
- [37] Kuipers J B 1999 *Quaternions and Rotation Sequences* (Princeton, NJ: Princeton university press)
- [38] Keller H U, Richter K and Thomas G E 1981 Multiple scattering of solar resonance radiation in the nearby interstellar medium. II. *Astron. Astrophys.* **102** 415
- [39] Brandt J C and Chamberlain J W 1959 Interplanetary gas. I. hydrogen radiation in the night sky *Astrophys. J.* **130** 670
- [40] Fayock B, Zank G P and Heerikhuisen J 2013 Comparison of Pioneer 10, Voyager 1, and Voyager 2 ultraviolet observations with anti-solar lyman-alpha backscatter simulations *Astrophys. J.* **775** L4
- [41] Hall D T 1992 *Ultraviolet resonance radiation and the structure of the heliosphere* Ph.D. thesis Arizona University in Tucson
- [42] Quémerais E and Bertaux J-L 1993 Radiative transfer in the interplanetary medium at Lyman alpha *Astron. Astrophys.* **277** 283
- [43] Scherer H and Fahr H J 1996 H Lyman alpha transport in the heliosphere based on an expansion into scattering hierarchies *Astron. Astrophys.* **309** 957
- [44] Gangopadhyay P, Ogawa H S, and Judge D L 1989 Evidence of a nearby solar wind shock as obtained from distant Pioneer 10 ultraviolet glow data *Astrophys. J.* **336** 1012
- [45] Hummer D G 1962 Non-coherent scattering: I. The redistribution function with Doppler broadening *Mon. Not. Roy. Astron. Soc.* **125** 21